JOURNAL OF GEOPHYSICAL RESEARCH, VOL. 112, D12201, doi:10.1029/2006JD008238, 2007

A case study of a frontal system simulated by a climate model: Clouds and radiation

Jingbo Wu,[1] Minghua Zhang,[1] and Wuyin Lin[1]

Received 9 November 2006; revised 15 February 2007; accepted 13 April 2007; published 16 June 2007.

[1] A case study is carried out to evaluate the capability of the Community Atmosphere Model (CAM3) in simulating frontal clouds over the Southern Great Plains (SGP). It focuses on a midlatitude cyclonic storm system observed during the March 2000 Intensive Observation Period (IOP) of the Atmospheric Radiation Measurement Program (ARM). Cloud biases are found to be consistent with climate model biases in this region: overestimation of optically thick clouds and shortwave cooling at the top-of-the-atmosphere (TOA), underestimation of optically thin middle clouds. Satellite observations, NOAA ETA analysis and a suite of ARM measurements are used to analyze the model cloud biases. We found two independent causes of model errors during two stages of the evolution of the cyclone. In the first stage, the biases are from cloud microphysical properties. The model significantly overpredicted cloud liquid water path, while it underpredicted cloud ice water path. As a result, it overestimated the magnitude of shortwave cloud forcing. In the second stage, the model cloud biases are primarily caused by a faster eastward propagation of the 500 mbar ridge behind the cyclone, which dissipated the high- and middle-level clouds but favored low clouds, leading to biases in cloud forcing. Averaged over the cyclone domain and period, the model simulated shortwave and longwave TOA cloud forcing of -113 W/m^2 and 30 W/m^2, respectively, while the corresponding observations are -69 W/m^2 and 38 W/m^2. Our results illustrated the feasibility of using synoptic cases to understand and eventually eliminate systematic cloud biases in climate models.

Citation: Wu, J., M. Zhang, and W. Lin (2007), A case study of a frontal system simulated by a climate model: Clouds and radiation, *J. Geophys. Res.*, *112*, D12201, doi:10.1029/2006JD008238.

1. Introduction

[2] *Cess et al.* [1990] found a roughly threefold variation in one measure of global climate sensitivity among 19 models attributable to differences in the models' depiction of cloud feedback. Despite the decade-long effort to improve the reliability of General Circulation Model (GCM) simulations of regional and long-term climate changes, however, cloud-climate feedback remains to be one of the greatest uncertainties [*Cubasch et al.*, 2001]. Further work needs to be done to improve the treatment of clouds in GCMs to make their projections for future climate change more accurate [*Bony et al.*, 2006].

[3] Several recent studies identified systematic cloud biases in climate models [*Webb et al.*, 2001; *Norris and Weaver*, 2001; *Tselioudis and Jakob*, 2002; *Lin and Zhang*, 2004; *Zhang et al.*, 2005]. The two major biases common in most models are the overestimation of optically thick clouds and significant underestimation of optical thin and medium low and middle clouds in the model. These biases exist in both tropics and in the middle latitude storm tracks. They cast doubt on the reliability of simulating cloud feedback processes in the models.

[4] Clouds have lifetimes of minutes or hours to at most a few days. Consequently it is appropriate to examine cloud-related processes on these timescales. Sources of model errors can be from inappropriate cloud parameterization, or poor simulation of the large-scale circulation and its moisture transport, or incorrect feedbacks between the large-scale circulation and the cloud parameterization on these timescales. Since one of the largest errors in GCM cloud simulations is from midlatitude synoptic-scale frontal cloud systems [*Lin and Zhang*, 2004; *Zhang et al.*, 2005], this study focuses on frontal clouds in GCMs.

[5] There have been steady improvements in forecasting extratropical cyclogenesis in the operational models as a direct result of (1) improvements in the numerical models with higher resolution, (2) more sophisticated treatment of physical processes, (3) model-based data assimilation systems, and (4) the increasing power of the computers that could be applied to the integration of the full set of predictive equations [*Uccellini et al.*, 1999]. A series of papers by *Junker et al.* [1989], *Sanders and Auciello* [1989], *Mullen and Smith* [1990], *Sanders* [1992], *Grumm et al.* [1992], *Smith and Mullen* [1993], *Oravec and Grumm* [1993] and *Grumm* [1993] all point to the increasing skill

[1]Institute for Terrestrial and Planetary Atmospheres, Marine Sciences Research Center, Stony Brook University, State University of New York, Stony Brook, New York, USA.

0148-0227/07/2006JD008238$09.00

of the National Meteorological Center (NMC) operational global and regional models over the 80s and 90s in predicting cyclogenesis. Despite the extensive research on operational models' performance in predicting the cyclogenesis, the performance of these models in predicting clouds associated with the extratropical cyclones is largely unexplored. Performances of climate models in simulating these clouds at coarse resolutions are also largely unknown. The few exceptions are statistical comparison between climatological output with observations or compositing studies [*Klein and Jakob*, 1999; *Norris and Weaver*, 2001; *Tselioudis and Jakob*, 2002]. Case studies are used by *Katzfey and Ryan* [1997, 2000] and *Ryan et al.* [2000]. Their results pointed out the importance of the subgrid-scale dynamics in simulating the frontal circulation and clouds, but many questions remain open.

[6] The present study attempts to reveal the causes of climate model biases at the process level through a synoptic case so that insights can be gained to guide future model improvement efforts. A special requirement for a climate model to carry out a case study is the initialization of the model with observed conditions so that its results can be compared with observations. This approach is used in the present investigation. The March 2000 SGP cyclone case is selected for two reasons: a large amount of cloud data is available with high temporal resolution, and SCM/CRM (Single-Column Models and Cloud Resolving Models) results with prescribed forcing are available from the ARM/GCSS case study as references. The objectives of this study are twofold: (1) to examine biases in simulated frontal clouds in the CAM3 that could be relevant to the model systematic errors and (2) to investigate the causes of the cloud biases during the event.

2. Data and Models

2.1. Data

[7] The observations are centered on the ARM SGP site from 1 March to 4 March 2000 when a frontal system passed through the Oklahoma and Kansas region. Three types of data are constructed. One involves the spatial and temporal structure of the atmospheric dynamics and thermodynamics. The second is for clouds. The third involves radiation.

[8] The ETA (NCEP's Limited Area Step Mountain Coordinate Model) three-dimensional analysis is used to characterize the regional structures of the frontal system. The data is from the 3 hourly operational NCEP ETA 212 grid (CONUS 212 grid, NCEP Office Note 388: GRIB, Table B Grid Identification, available at http://www.nco.ncep.noaa.gov/pmb/docs/on388/) with 40 km horizontal resolution and 26 pressure levels in the vertical. The NCEP Global Final Analyses (FNL) is used when large-scale atmospheric conditions are needed for model initialization and forcing. The FNL analysis is available every 6 hours and with $1.0 \times 1.0^\circ$ resolution at 26 mandatory levels from 1000 mbar to 10 mbar. In addition, the variational analysis of vertical velocity at the ARM SGP site is also used [*Zhang and Lin*, 1997; *Zhang et al.*, 2001]. This analysis was derived from a special network of coordinated 3-hourly sounding along with a network of six wind profilers centered around the ARM SGP with additional mass, energy, and moisture constraints.

[9] For the evaluation of model clouds, the (GOES) data are used for the cloud horizontal patterns; the ARM Active Remote Sensing of Clouds (ARSCL) cloud product [*Clothiaux et al.*, 2000] and the ARM MICRO-BASE cloud product [*Miller et al.*, 2003; *U.S. Department of Energy*, 2006] at the ARM SGP central facility (CF) are used for the cloud vertical structures. Three GOES products are employed. The first one is the gridded data with cloud properties derived at NASA Langley Research Center from the LBTM algorithm and from the VISST algorithm [*Minnis et al.*, 1995]. It covers an area of $13.5^\circ \times 9.5^\circ$ in longitude and in latitude respectively centered on (37°N, 98°W) with 0.5° resolution in both directions. Available variables in this product include cloud fractions and cloud top temperatures of total cloud, and the separate high-, middle-, and low-level clouds, as well as cloud liquid water path and cloud ice water path. Clouds with satellite-derived cloud top between 2 and 6 km are classified as middle-level clouds; high-level clouds have cloud tops above this range, and low-level clouds have cloud tops below this range. The sum of the high-, middle- and low-level cloud fraction does not exceed 100%. The cloud fraction is as viewed from top of the atmosphere. One therefore needs to bear in mind that middle and low clouds represent the actual distribution only when they are not obstructed by clouds above.

[10] Since the horizontal domain of the above GOES product is too small to cover the whole cyclone system, a second GOES product is used. It is the infrared brightness temperature from channel 4 which were collected and preprocessed by SeaSpace. The area is from 24.33°N to 47.26°N and 89.65°W to 105.31°W centered at the SGP CF (36.605°N, 97.485°W). The pixel size (horizontal resolution) is 4 km. There are 350×640 pixels in the covered domain. The satellite brightness temperatures are compared with the modeled cloud top temperatures.

[11] The third satellite data set is from the International Satellite Cloud Climatology Project (ISCCP). The ISCCP D1 radiative flux data are used to estimate the cloud radiative forcing of the frontal clouds in this case study. The product contains 3-hourly full-sky and clear-sky shortwave and longwave, upwelling and downwelling fluxes at five vertical levels including surface and top-of-atmosphere (TOA) [*Zhang et al.*, 2004].

[12] The ARM ARSCL cloud product is from a combination of radar data and lidar estimates measurements [*Clothiaux et al.*, 2000, 2001]. It contains the best estimate of the vertical locations of the cloud hydrometeors above the ARM SGP site. The original data has a temporal resolution of 10 s and a vertical height resolution of 45 m. The cloudiness occurrence used in this study has been mapped to a vertical pressure coordinate with 25 mbar resolution. The MICRO-BASE product [*Miller et al.*, 2003; *U.S. Department of Energy*, 2006] provides the cloud liquid and ice water contents over the ARM SGP CF. Both the ARSCL and the MICRO-BASE cloud products are only available at the single station of the ARM SGP site. In this case study, we used the point radar column measurements to compare with the model results representing averages over 280 km wide grid box. The mismatch in temporal and spatial sampling between the radar and model grid represents an incompatibility for model data comparison. On the basis of the GOES satellite figure and the simulated cloud

shield, we expect this mismatch to be smaller after time averaging of the radar data to 3 hours. The temporal average of 3-hour is used to represent space averages over a model grid.

[13] In our discussions, the atmospheric dynamic and thermodynamic structures, clouds, and the radiation fields are organized to present a coupled dynamics-physics frontal system. They are then compared with model results.

2.2. Model

[14] The CAM3 used in this study is the version 3.0 atmospheric model of the Community Climate System Model (CCSM3) [*Collins et al.*, 2006]. The novel application of CAM3 is that the simulations are initialized with operational analysis. This allows us to carry out case studies so that simulated atmospheric fields can be directly compared with measurements. The initialization package of the model was developed by Wuyin Lin at Stony Brook University. It is similar to the current Climate Change Prediction Programs–ARM Parameterization Testbed design (CAPT) (http://www-pcmdi.llnl.gov/projects/capt/). *Boyle et al.* [2005] described in detail how the model was initialized in CAPT. In this study, CAM3 was initialized at 6Z 1 March 2000 using the FNL global analysis and the NCEP OI global sea surface temperature (SST). The land surface model was initialized using FNL data. The $1^\circ \times 1^\circ$ OISST data is also used as the ocean surface condition throughout the integration. The horizontal resolution is T42 ($2.8^\circ \times 2.8^\circ$ grid). There are 26 vertical levels with the top at 3.5 hPa. The time step is 20 min. It was integrated for 3 days. For humidity above 100 mbar, climatology derived from SAGE II (Stratospheric Aerosol and Gas Experiment II) is used.

[15] CAM3 employs the prognostic cloud microphysical scheme of *Rasch and Kristjánsson* [1998] with the fractional stratiform condensation scheme of *Zhang et al.* [2003]. Cloud amount is parameterized on the basis of three factors: relative humidity, convective mass fluxes, and strength of surface inversion. Only the first factor is important for the stratiform clouds that are the focus of the present study. The fractional condensation closure introduced by *Zhang et al.* [2003] has eliminated the possibility of the model diagnosing cloud amount while having no hydrometeors or vice versa for stratiform clouds. In this sense, it is equivalent to the more modern cloud schemes that are based on the probability distribution function of total water content.

[16] The cloud overlap for radiative calculations in CAM 3.0 is maximum-random. Clouds in adjacent layers are maximally overlapped, and groups of clouds separated by one or more clear layers are randomly overlapped. For diagnostic purposes, the CAM 3.0 calculates three levels of cloud fraction assuming the same maximum-random overlap as in the radiative calculations. These diagnostics, denoted as low, middle, and high cloud, are bounded by the pressure levels from surface to 700 mbar, 700 mbar to 400 mbar, and 400 mbar to the model top. In our case study, the simulated low-, middle-, and high-level clouds were directly compared with the GOES satellite cloud products. For this particular case, the differences between the model and the data were mainly "no cloud" versus "clouds," which makes it unnecessary to further construct model clouds using a satellite algorithm such as the ISCCP simulator.

3. Results

3.1. Observations

[17] The 1–4 March 2000 frontal cloud simulation was also the subject of the ARM-GCSS Case 4 study. *Xie et al.* [2005] described the evolution of the system and cloud simulations in single-column models and cloud resolving models in which prescribed large-scale forcing at the ARM SGP were used. Starting at 12Z 1 March 2000 (hereinafter, the date and time will be referred as 1/12 and so on with the month and year omitted), a cyclone and a cold front developed over Arizona. The system then progressed eastward into a low-pressure region with a preexisting stationary front over central Texas and became a fully developed cyclone-frontal system.

[18] Figure 1 shows the synoptic condition over the SGP at 3/0 associated with the mature cyclone. Near the surface (Figure 1a), the center of the low is in northern Texas. The ARM SGP is under the influence of the warm front associated with the cyclone, which is manifested both in the large surface temperature gradient over the southern border of Oklahoma and in the southerly to northeasterly wind shear in Oklahoma. At 850 mbar (Figure 1b), the southerly wind in Oklahoma penetrated northward, representing the spreading of warm air over the 1000 mbar northeasterly flow. The warm and cold fronts occluded below 500 mbar, where the system is characterized by a baroclinic synoptic wave with a closed low (Figure 1c). The center of the low tilted slightly northwestward with altitude.

[19] Figures 2a and 2b show the initial condition of the 700 mbar height at 1/6 and its distribution at 3/0 when the cyclone is developed. The GOES8 infrared brightness temperature is superimposed on the ETA 700 mbar geopotential height field at 3/0. The cloud shield has the typical comma shape associated with a cyclone [*Carlson*, 1980]. The comma tail and head can be identified clearly. The ARM cloud radar was located at the border of Oklahoma and Kansas (shown with a red dot).

[20] Figure 2c shows the vertical structure of clouds as measured by the cloud radar at the ARM SGP site. When the cloud system moved over the ARM SGP site, the radar first measured clouds with their bottom descending as the warm front approached. The cloud maximum of a deep layer cloud is then observed. This is followed by a cloud minimum due to the dry intrusion from behind the upper level trough. Finally, a second cloud maximum is measured from the west protrusion part of the comma head. Middle and high clouds continue to be present for most of day on 4 March when the system still remains near the SGP region.

3.2. CAM3 Simulations

[21] The simulated development of the cyclone and clouds in the CAM3, corresponding to observations in Figures 2a and 2b, is shown in Figures 3a and 3b. The model successfully calculated the development and the location of the 700 mbar cyclone by 3/0 with lead time of 42 hours. As can be expected, the simulated cyclone

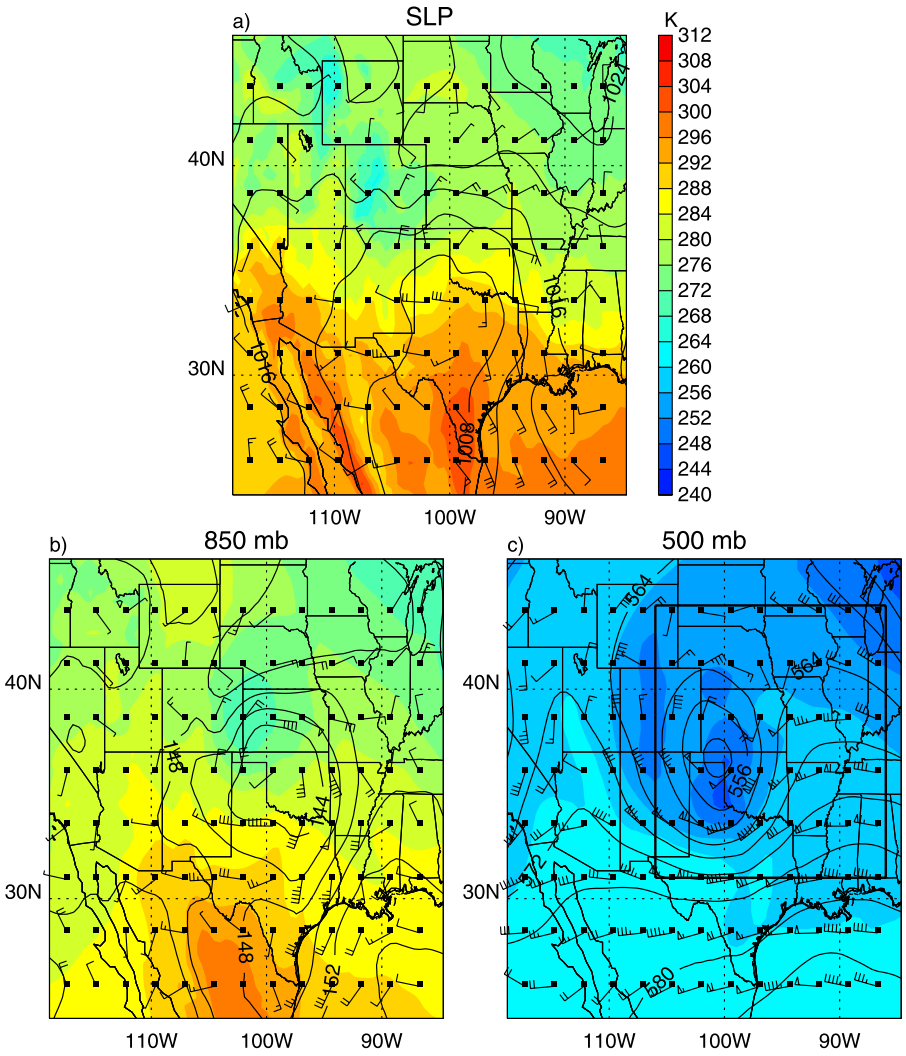

Figure 1. Synoptic configuration at 0Z 3 March 2000: (a) sea level pressure (hPa), surface temperatures (°K), and 1000 hPa wind fields; (b) geopotential height contours (10 m), temperatures (°K), and wind fields at 850 mbar; and (c) geopotential height contours (10 m), temperatures (°K), and wind fields at 500 mbar. Black box shows the cyclone area over which the domain average cloud radiative forcing is calculated. Contours are drawn every 40 m at 500 mbar, every 20 m at 850 mbar, and every 4 hPa at sea level. Temperatures are drawn every 4°K. One barb in wind symbol means 4 m/s. One triangle in wind symbol means 20 m/s.

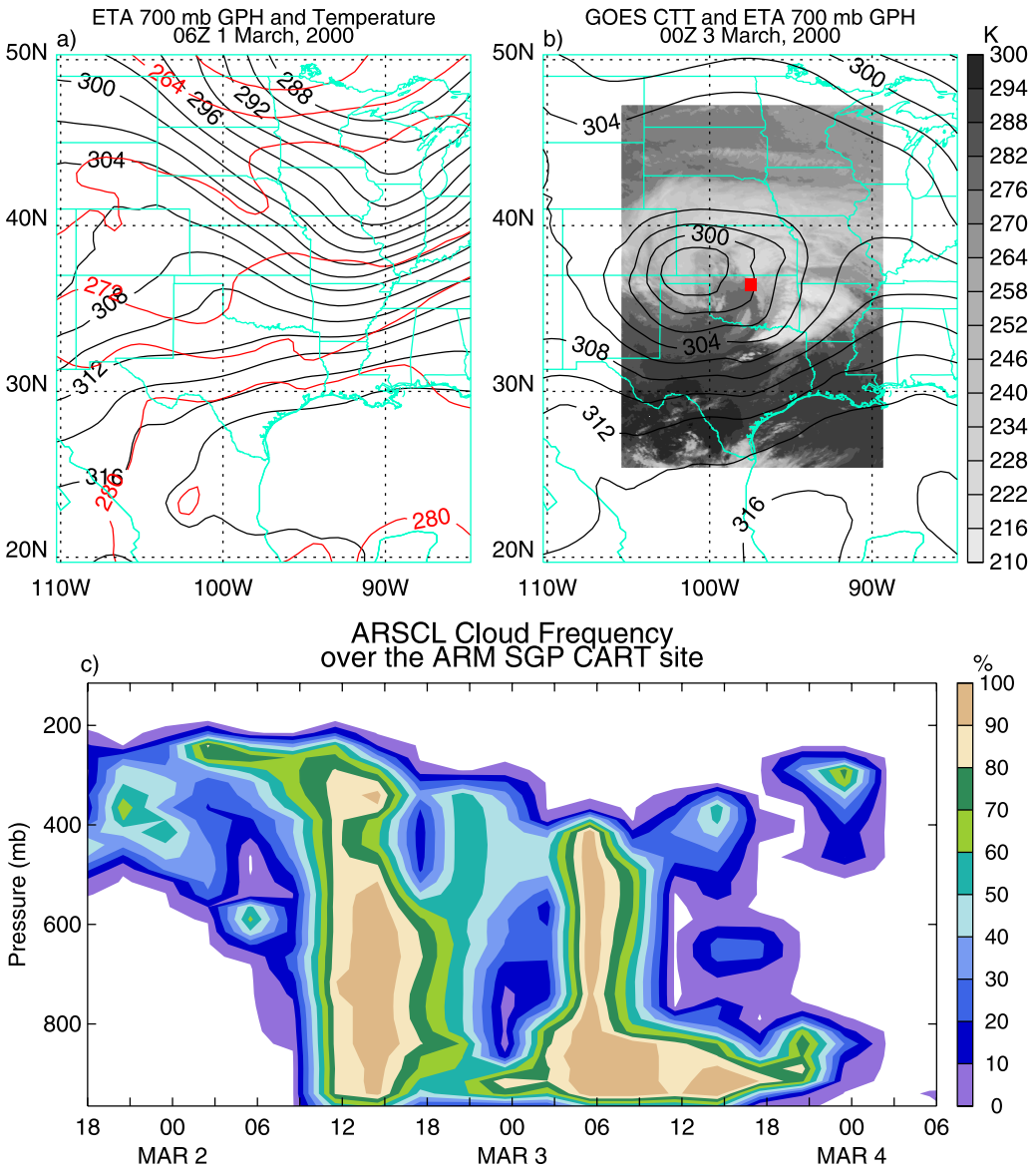

Figure 2. (a) ETA 700 mbar temperature (°K) and geopotential heights (10 m) at 0Z 1 March 2000, (b) GOES infrared temperature (°K) and 700 mbar geopotential heights (10 m) from ETA analysis at 0Z 3 March 2000, and (c) ARSCL VAP cloud occurrence frequency (%) at the ARM SGP CF from 18Z 1 March to 6Z 4 March 2000. Geopotential height contours are drawn every 20 m. Red dot shows the location of the ARM SGP CF.

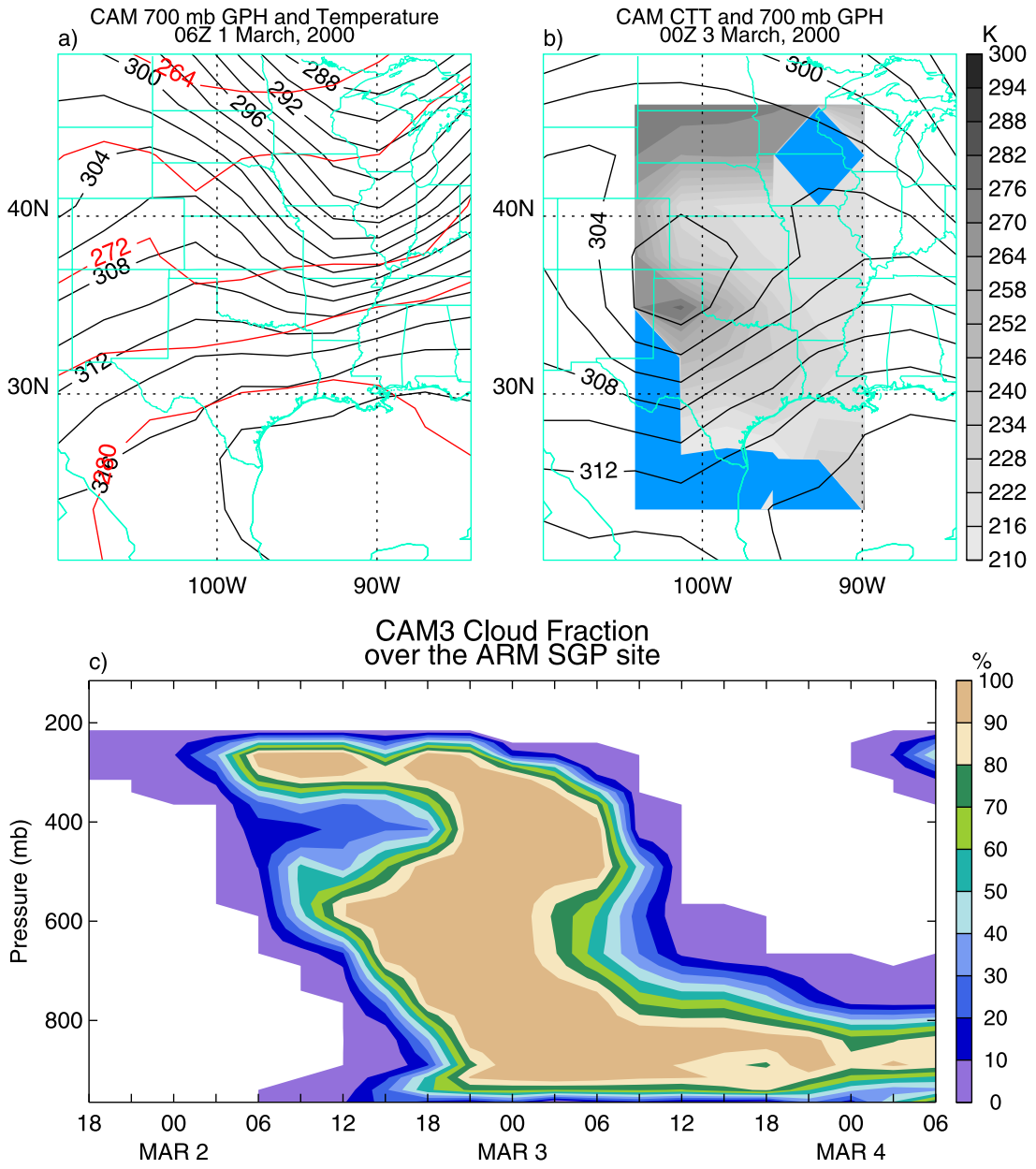

Figure 3. (a) CAM3 700 mbar temperature (°K) and geopotential height (10 m) at 0Z 1 March 2000, (b) CAM3 cloud top temperature (°K) and 700 mbar geopotential heights (10 m) at 0Z 3 March 2000, and (c) CAM3 cloud fraction (%) at the ARM SGP CF from 18Z 1 March to 6Z 4 March 2000. Geopotential height contours are drawn every 20 m.

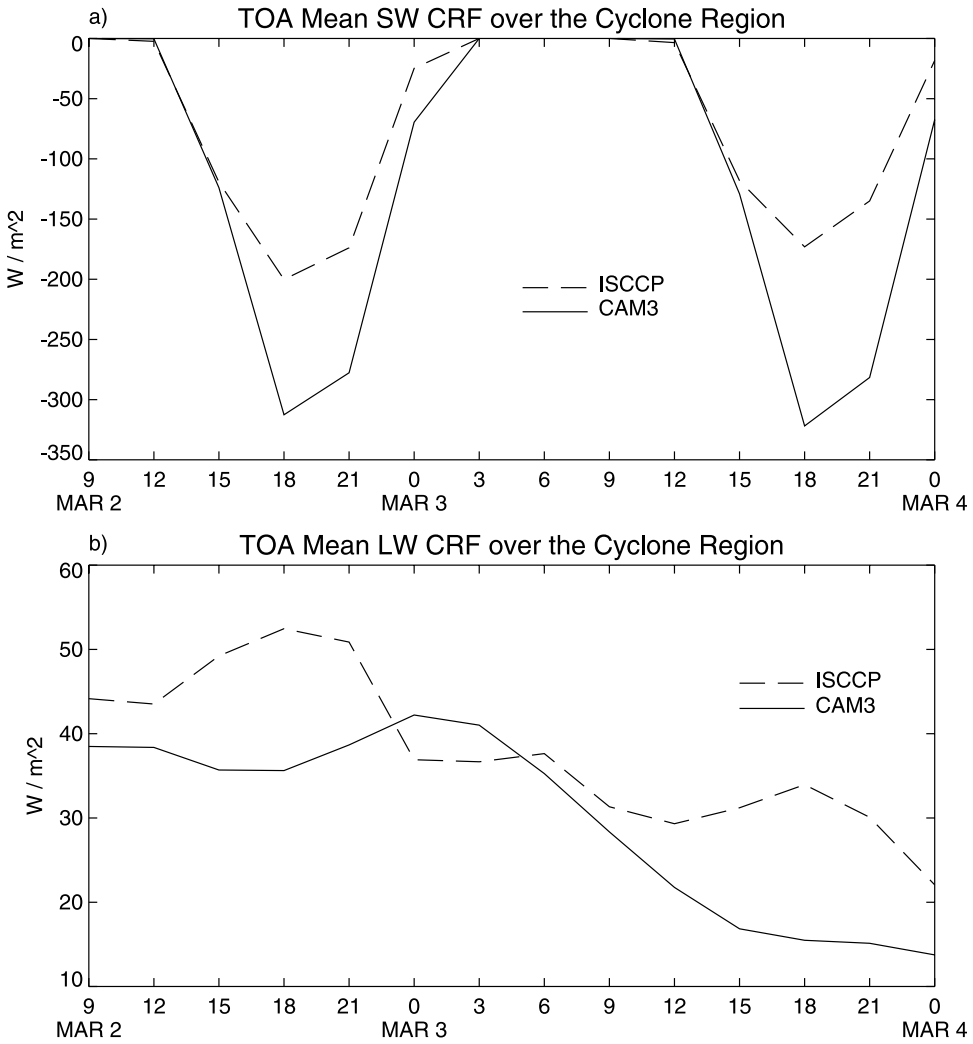

Figure 4. Cloud radiative forcing (W/m^2) from CAM3 and ISCCP for the period from 9Z 2 March to 0Z 4 March 2000: (a) mean SW CRF at TOA averaged over the cyclone region and (b) mean LW CRF at TOA averaged over the cyclone region.

intensity is weaker than in the ETA analysis owing to the coarse resolution of the GCM. The model simulated a broad cloud deck in front of the 700 mbar trough. Figure 3c shows the time-pressure cross section of cloud fraction from the CAM3 that corresponds to the radar measurements in Figure 2c. The model simulated the descending of the warm frontal cloud. It however maintained a deep layer of cloud for longer time at the SGP site; it missed the cloud break at the beginning of 3 March because of the dry intrusion; it missed the middle and high clouds after 3/12, but overestimated low clouds after that.

[22] GCMs are not meant to capture the fine structures of the observed cloud features. We therefore focus on the domain-averaged cloud-radiative forcing, an unambiguously defined physical quantity, over the frontal system during the event. The domain is defined from 31°N to 44°N and from 106°W to 86°W (black box as in Figure 1c), large enough to cover the cyclone but exclude other weather systems. The solid line in Figure 4a shows the model-simulated Top-of-Atmosphere (TOA) shortwave cloud forcing (SW CRF). The dashed line in Figure 4a is from ISCCP. It is seen that the model significantly overestimated the magnitude of the SW CRF. The biases on 2 and 3 March will be shown later as due to two completely different reasons. When averaged over the period shown in Figure 4a, the simulated SW CRF is -113 W/m^2 versus -69 W/m^2 in ISCCP.

[23] The corresponding comparison of the LW CRF between the CAM3 simulation and ISCCP data is shown in Figure 4b. LW CRF is underestimated in the model except for the first five hours on 3 March. During these hours, the overestimation of both the LW CRF and SW CRF is caused by the overestimation of the cloud amount (broad cloud deck in front of the 700 mbar trough in Figure 3b) which as expected is due to the lack of dry intrusion in the coarse resolution GCM. When averaged over the period shown in Figure 4b, the domain averaged LW CRF in the model is 30 W/m^2 versus 38 W/m^2 in ISCCP. Combining

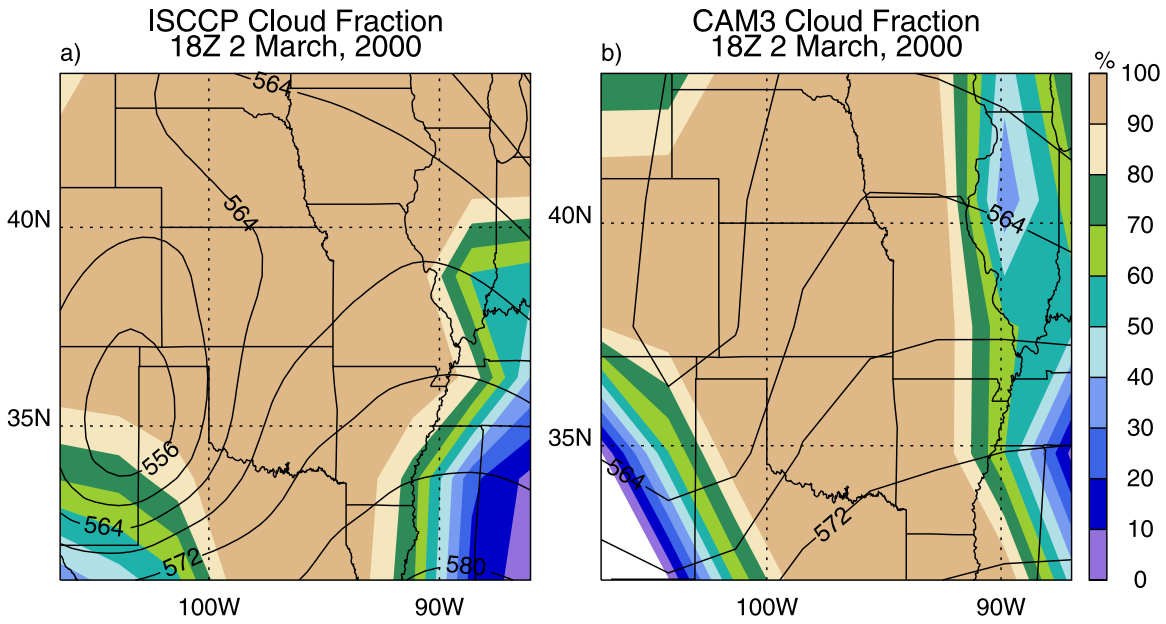

Figure 5. Total cloud fraction (%) at 18Z 2 March 2000: (a) CAM3 total cloud fraction and 500 mbar geopotential height (10 m) and (b) ISCCP total cloud fraction and 500 mbar ETA geopotential height (10 m). Geopotential height contours are drawn every 40 m.

the LW CRF with the SW CRF, the model simulated a net CRF cooling of -83 W/m^2 versus -31 W/m^2 in ISCCP, 2.5 times as strong as in the ISCCP data.

[24] The overestimation of the SW CRF is a general feature of the CAM in storm tracks [*Lin and Zhang*, 2004]. The underestimation of the LW CRF is however specific to the present case. On 3 March, the underestimation of the LW CRF is mainly due to the lack of postfrontal middle clouds as will be shown later.

[25] On 2 March, the simulated cloud amount was similar to ISCCP, or even slightly less in CAM3, although the simulated solar reflection is larger. Figure 5 shows the cloud amount comparison on 2/18. Total cloud amount therefore is not the cause of the CRF differences. Figures 6a and 6b show the cloud liquid water path (LWP) in the GOES observation and in CAM3 respectively at the same time on 2/18. It is seen that the model considerably overestimated the cloud liquid water path. Meanwhile, it significantly underestimated the cloud ice water path (IWP) as shown in Figures 6c and 6d. For the GOES data, cloud phase is determined by comparing the ratios of reflectance at two wavelengths: one that is a conservative scatterer for both ice and water and one that has strong absorption for ice and weak absorption for water [*Minnis et al.*, 1995]. The model partition of ice-liquid relies on a temperature threshold. This is part of the model parameterization that enters into the radiative calculation, and so the comparison helps to trace the causes of the radiation errors. In CAM3, liquid cloud particles are assumed to have sizes ranging from 8 micrometers to 14 micrometers depending on temperature. Ice cloud particles however are about an order of magnitude larger because of aggregation. For solar radiation, given the same condensate path, the small liquid particles are much more effective in scattering solar radiation back to space. As a result, the large percentage of LWP over IWP in the CAM3 relative to that in satellite data leads to overestimation of SW cooling in the model. The model underestimated LW warming to a lesser degree. At the single site of SGP, the difference of LW CRF between the model and observation is consistent with that for the cloud top height (CTH) (figure not shown). We therefore expect that the slight underestimation of LW CRF over the cyclone domain on 2 March is also due to the overall lower CTH in the model.

[26] In contrast to the cloud property bias on 2 March, the model bias on 3 March can be largely attributed to the different vertical distribution of cloud amount between the model and the satellite data. Figures 7a and 7b show the satellite measurements of high and middle clouds at 3/15. The corresponding simulation in the CAM3 is shown in Figures 7c and 7d. Superimposed on these figures are the 300 mbar and 500 mbar geopotential heights. It is seen that the underestimation of high and middle clouds is primarily caused by errors in the large-scale synoptic condition: the high-pressure ridge behind the cyclone moved eastward to the SGP earlier in the model.

[27] Figures 8a and 8b show the total and low cloud amount at 4/0 from GOES superimposed on the 500 geopotential height and sea level pressure respectively. At that time, the low-pressure center at sea level has moved out of Oklahoma. The SGP is under the influence of a high-pressure center. There is therefore very little low cloud. In the CAM3 simulation however (Figures 8c and 8d), because of the faster movement of the 500 mbar ridge and the associated surface high to the east, Oklahoma is already under the influence of the surface low-pressure system located at the south and to the west. As a result, the model simulated a large amount of low clouds. The overestimated low clouds and underestimated high clouds in the model on 3 March thus lead to the overestimation of shortwave cooling, and underestimation of the longwave cloud forcing.

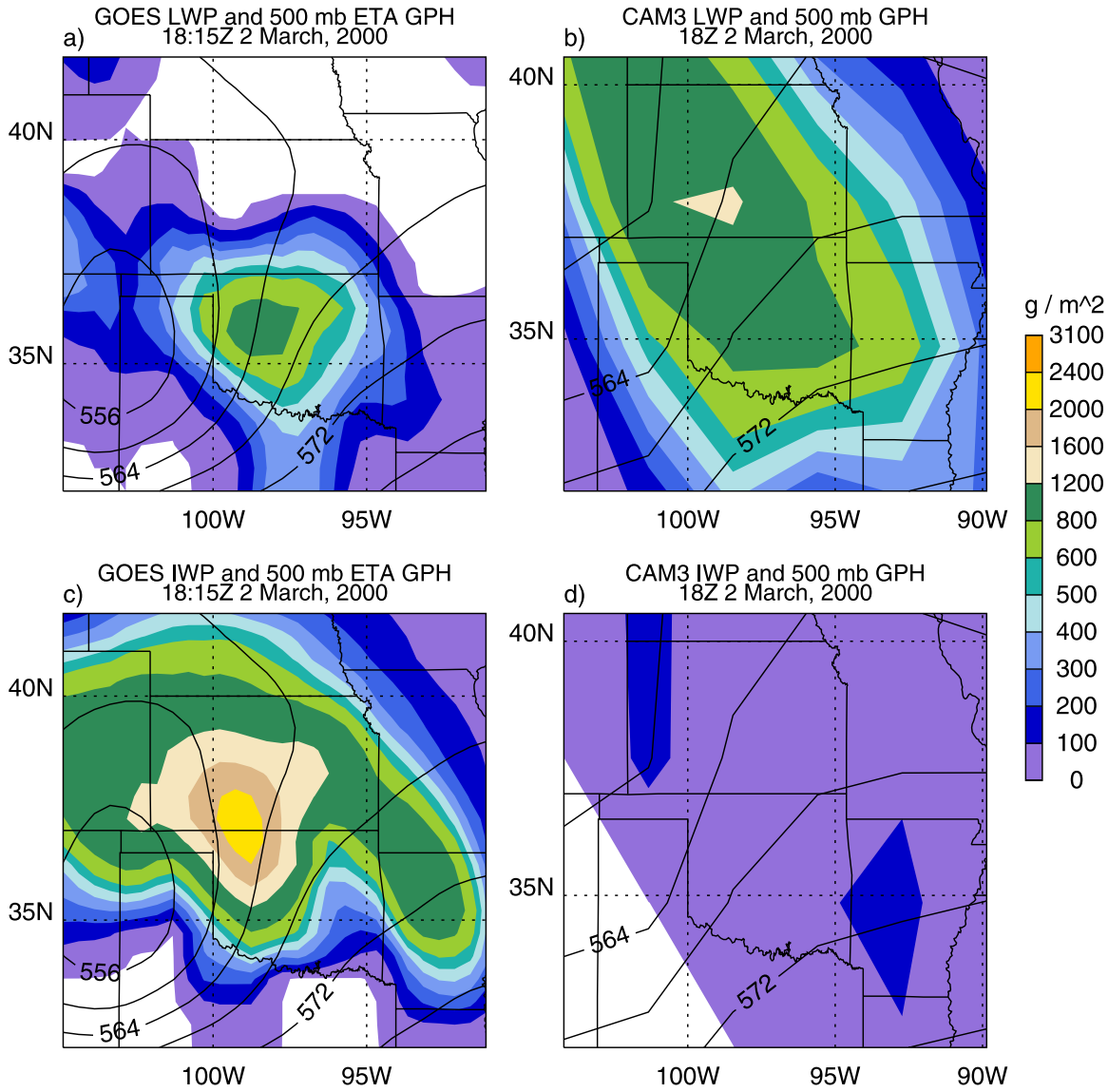

Figure 6. Cloud liquid water path (g/m^2) and cloud ice water path (g/m^2) at 18Z 2 March 2000 from GOES and CAM3: (a) GOES cloud LWP with 500 mbar ETA GPH at 2/18:15, (b) CAM3 cloud LWP and 500 mbar GPH at 2/18, (c) GOES cloud IWP with 500 mbar ETA GPH at 2/18:15, and d) CAM3 cloud IWP with 500 mbar GPH. Geopotential height contours are drawn every 40 m.

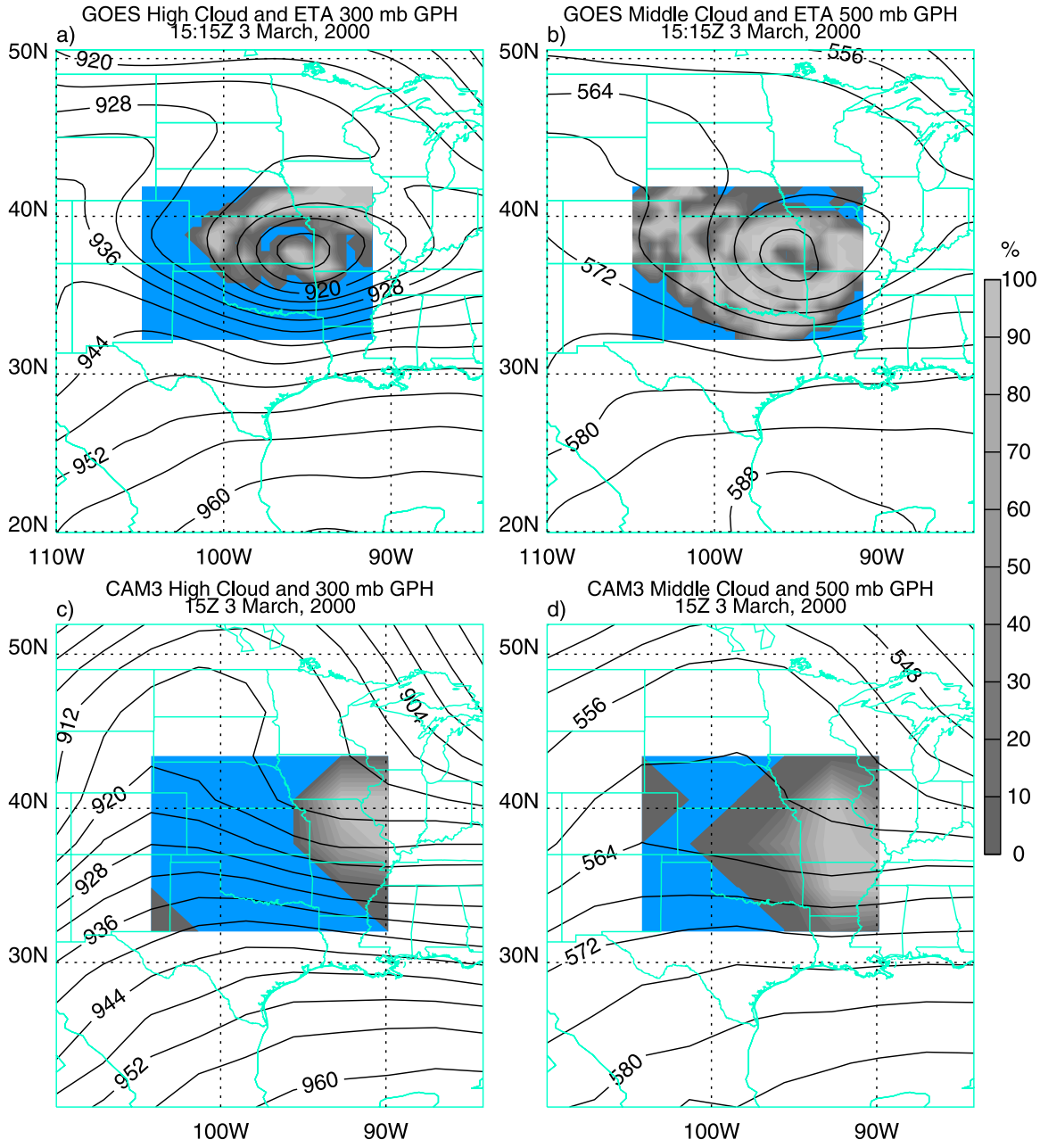

Figure 7. Cloud fraction (%) and GPH (10 m) around 15Z 3 March 2000: (a) GOES high-level cloud fraction and ETA 300 mbar GPH, (b) GOES middle-level cloud fraction and ETA 500 mbar GPH, (c) CAM3 high-level cloud fraction and 300 mbar GPH, and (d) CAM3 middle-level cloud fraction and 500 mbar GPH. Contours are drawn every 40 m.

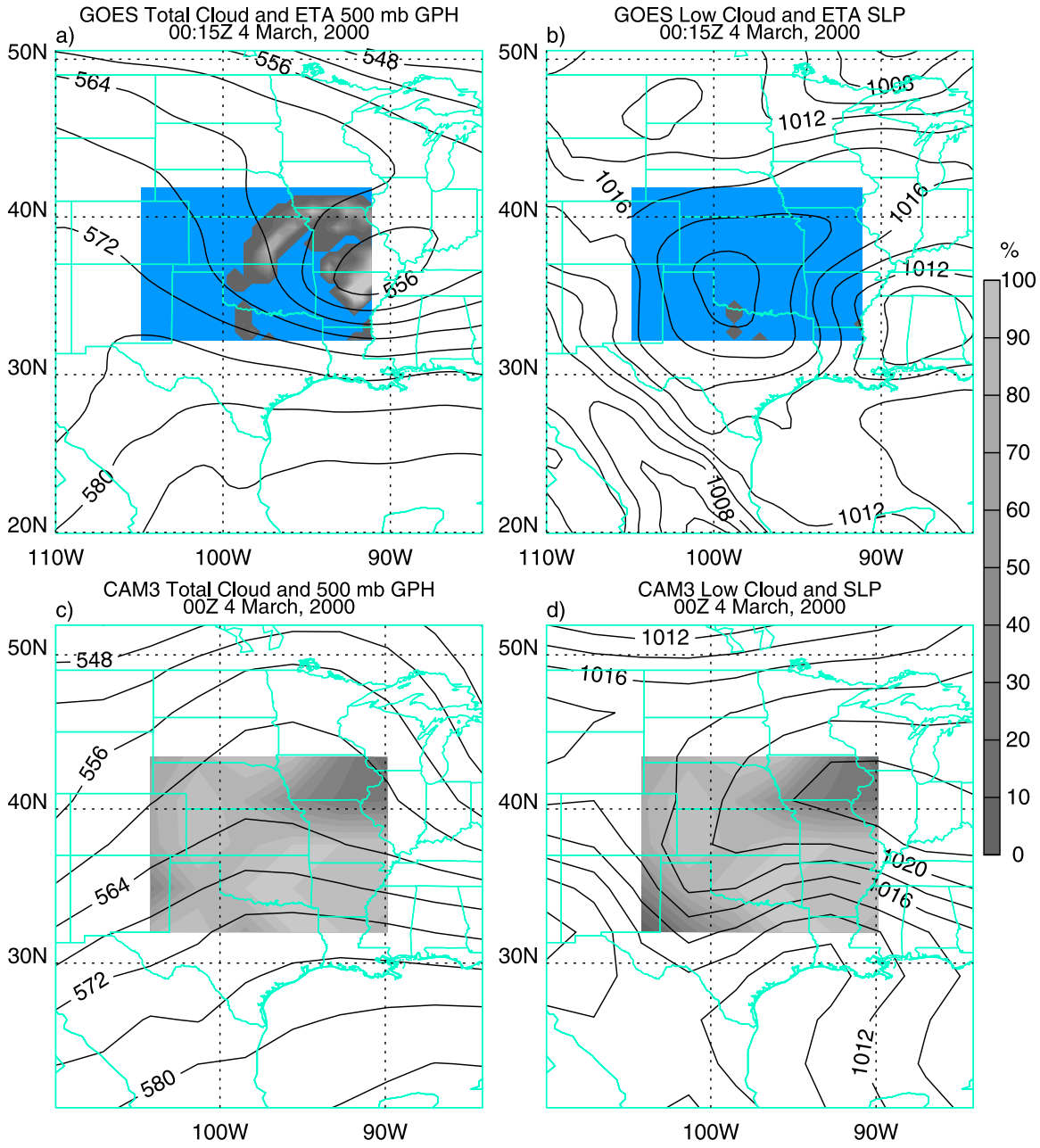

Figure 8. Cloud fraction (%), GPH (10 m) and SLP (hPa) around 0Z 4 March 2000: (a) GOES total cloud fraction and ETA 500 mbar GPH, (b) GOES low-level cloud fraction and ETA sea level pressure, (c) CAM3 total cloud fraction and 500 mbar GPH, and (d) CAM3 low-level cloud fraction and sea level pressure. Geopotential height contours are drawn every 40 m. SLP contours are drawn every 2 hPa.

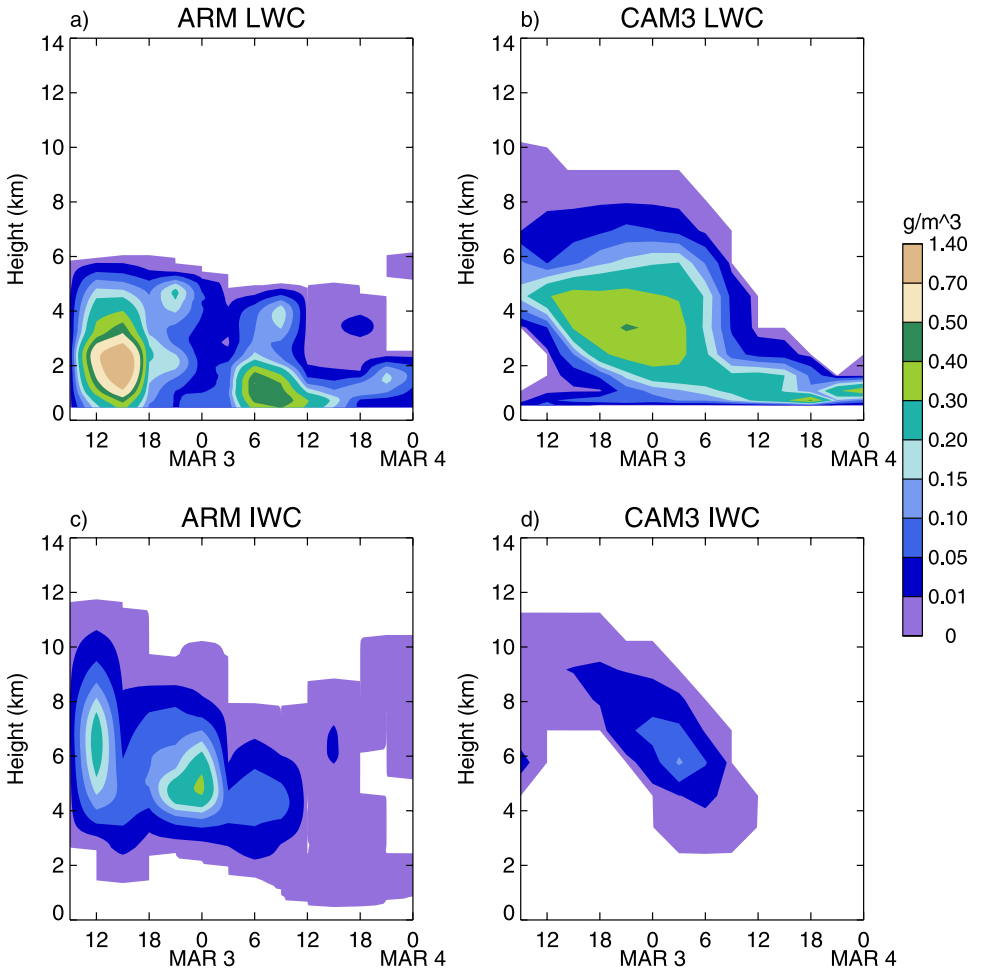

Figure 9. Time-pressure cross-section cloud water content over the ARM SGP site: (a) ARM cloud liquid content (g/m^3), (b) CAM3 cloud liquid content (g/m^3), (c) ARM cloud ice content (g/m^3), and (d) CAM3 cloud ice content.

[28] Because of potential uncertainties of satellite data, we also analyze the above model biases at the ARM SGP site. Even though we do not expect the model bias at a single grid point to replicate those of the cyclone domain averages, we wish to establish that the above two main causes of model biases are also present.

[29] Figures 9a and 9b compare the ARM MICRO-BASE data of cloud liquid water content with that simulated in the CAM3 at the SGP site. It is seen that the model also simulated considerably more cloud liquid amount, consistent with what was shown in Figures 6a and 6b for the cyclone domain using satellite data. Figures 9c and 9d show the comparison of simulated and ARM MICRO-BASE data of cloud ice water content that is also consistent with satellite data comparison in Figures 6c and 6d.

[30] The ARM continuous baseline microphysical retrieval (MICRO-BASE) VAP data was derived from a combination of observations from the millimeter cloud radar (MMCR), the ceilometer, the micropulse lidar (MPL), the microwave radiometer (MWR) and balloon-borne sounding profiles to determine the profiles of liquid/ice water content (L/IWC), liquid/ice cloud particle effective radius (re) and cloud fraction. The L/IWC is determined from the radar reflectivity values in the ARSCL VAP [*Clothiaux et al.*, 2000]. For liquid cloud layers ($T > 0°C$), LWC is calculated using the radar reflectivity – LWC relationship derived by *Liao and Sassen* [1994]. For ice cloud layers ($T \leq -16°C$), the IWC is determined using the Z-IWC relationship from *Liu and Illingworth* [2000]. For the mixed phase region of the cloud ($-16°C < T < 0°C$), it assumes a linear fraction of ice/liquid where the ice fraction is equal to $-T[°C]/16$ [*U.S. Department of Energy*, 2006]. In the CAM3, total condensate is partitioned into liquid and ice phases based on temperature following *Sundqvist* [1988]. Above $-10°C$, all condensate is assumed to be liquid; below $-40°C$ all are considered as ice. In between, the fraction is linearly interpolated with respect to temperature. Sedimentation, evaporation, and convective transport are separately calculated for the liquid and ice phases. Observations and more detailed microphysical models have reported wide range of ice to liquid ratios as functions of temperature, which are most likely related with geographical locations and the history of clouds. In this case study, the dynamical circulation and the intensity of vertical velocity between the model simulation and observations on 2 March are similar. Yet the microphysical properties of the clouds are very different.

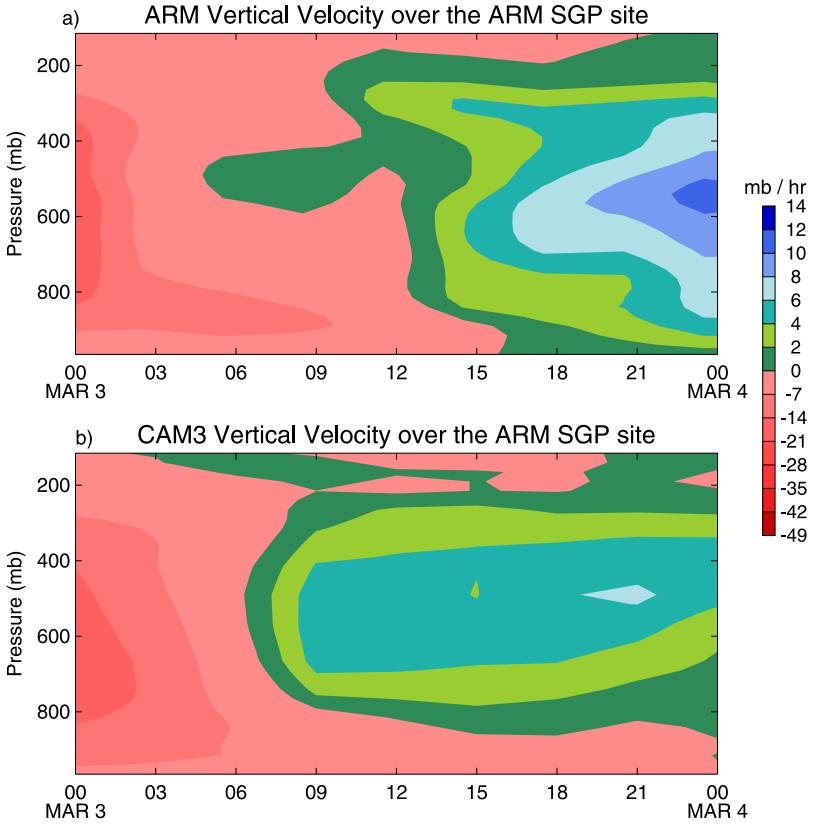

Figure 10. Time-pressure cross section of the vertical velocity (mbar/hour) over the ARM SGP domain for the period from around 0Z 3 March to 0Z 4 March 2000: (a) ARM variational analysis and (b) CAM3 simulation.

One plausible explanation is that the liquid-to-ice ratio is significantly overestimated in the CAM over the cyclone domain. The different assumption made to distinguish liquid/ice between the data and the model may have contributed to the biases between them. However, the difference should mainly represent that of the physical processes. It is conceivable that frontal systems tend to generate dust minerals that can serve as cloud ice nuclei at high temperatures. This is a topic worth of further study.

[31] To show the bias on 3 March, we use the vertical velocity fields at the SGP site in Figure 10. In Figure 10, red means upward motion, blue and green mean downward motion. When the model vertical velocity in Figure 10b is compared with the variationally analyzed vertical velocity in Figure 10a, the midtropospheric downward motion clearly begins earlier in the simulations. This is consistent with the previous analysis of the earlier arrival of the middle tropospheric ridge. Near the surface, the simulated upward motion also prevailed on the second half of 3 March. This is consistent with influence of surface low pressure in Figure 8d.

[32] Thus the sources of model biases in the cyclone domain are also seen at the ARM SGP site where independent data have been used. Namely, model errors in cloud microphysical properties dominated the first day of 2 March, and errors in dynamical circulations are responsible to biases on 3 March. In the work by *Xie et al.* [2005], single-column models were also shown to overestimate cloud liquid amount but underestimate the ice liquid path. The present case study using an initialized GCM allows us to demonstrate that the cloud microphysical biases extend to the cyclone domain averages in a GCM setting, and that additional errors are present because of biases in model dynamical circulations in the later stage of the cyclone.

[33] While the model is able to simulate the development and the location of the 3 March cyclone as in Figures 3a and 3b, it failed to calculate the correct propagation after the cyclone matures, which contributed to the cloud biases and cloud forcing fields in the later stage of the event. There are several possible reasons, including model physical parameterizations, errors in initial conditions, and so on. We have carried out a number of simulations with slightly different initial conditions. The results are similar to what have been reported in this paper. In a companion paper, we will show that the faster propagation of the high-pressure ridge in the CAM3 is due to the difference of effective stability between the model and data, i.e., the different cancellations between the diabatic heating and adiabatic cooling, which is further traced to the lack of subgrid-scale transport of vorticity and temperature advection in the GCM as a result of CAM's coarse resolution. It will also be shown that the inadequate simulation of the dry tongue associated with the cyclone is improved in the higher-resolution simulation.

3.3. Sensitivity

[34] The large biases in the simulated cloud hydrometeors on 2 March prompted us to carry out a sensitivity experiment by modifying the partitioning of the cloud liquid/ice in

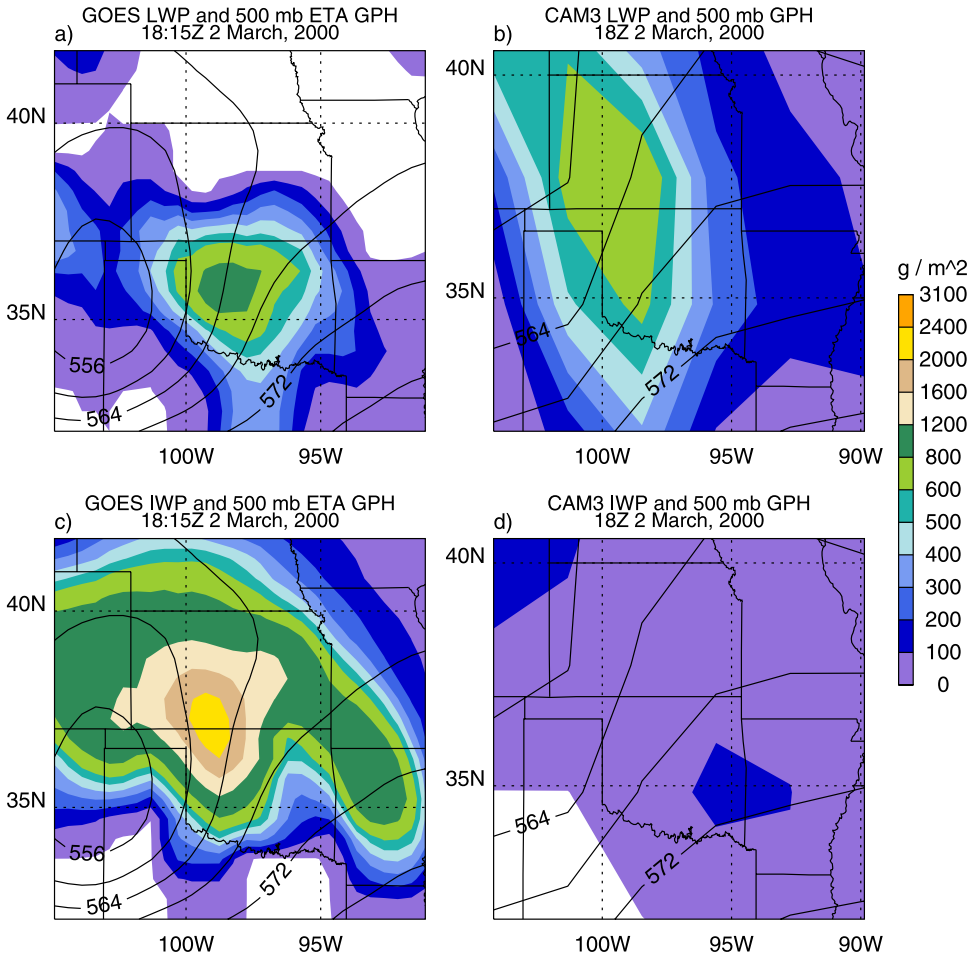

Figure 11. Same as Figure 6 except that CAM3 results are from sensitivity experiment.

the model following the way used in the MICRO-BASE retrievals. Cloud layers with temperatures between 0°C and −16°C are assumed to be mixed phase clouds with a linear fraction of ice/liquid where the ice fraction is equal to −T[°C]/16; cloud layers with temperatures below −16°C are assumed to have pure ice; and cloud layers with temperatures above 0°C are assumed to have pure liquid.

[35] The simulated cloud LWP/IWP distribution and corresponding satellite retrievals are shown in Figure 11. Comparing with the control run (Figure 6b and 6d), the simulated LWP reduced. However, the simulated IWP shows little change. The evolutions of simulated LWC/IWC over the ARM SGP site and the corresponding MICRO-BASE data are shown in Figure 12. Similarly, the simulated LWC reduced at high level, while the simulated IWC does not increase as much as the reduction of the LWC. These results suggest that the ice problem is very likely due to the ice microphysics scheme. The accretion rate and/or the conversion of ice to snow are likely too large.

4. Conclusion

[36] Frontal clouds associated with a cyclone have been simulated using CAM3 that passed through the ARM SGP during 1–3 March 2000 and have been evaluated against observations. We have shown that the model calculated the initial development and location of the cyclone. It however significantly overpredicted domain averaged cloud cooling effect but underpredicted the cloud-warming effect. This is because the model significantly overestimated the cloud liquid water path, but underestimated cloud ice water path, a source of error from the cloud microphysical property parameterizations. After the cyclone matures, the model simulated a faster eastward propagation of a high-pressure ridge behind the front, leading to earlier dissipation of middle to high clouds, and persistence of low clouds. This also resulted in overestimation of cloud shortwave cooling and underestimation of longwave warming. Averaged over the period, the domain averaged net cloud cooling in the CAM3 is 83 W/m^2 versus 31 W/m^2 in ISCCP during the event. Both biases are also confirmed using data from ground radar measurements from the ARM field campaign.

[37] The problem of overestimation of optically thick clouds in strong synoptic upward motion region has been identified as a generic problem in climate models. The consistency of the cloud bias in the CAM3 case study and climate model statistical analysis indicates that synoptic cases are able to provide some insights to the statistical results. The effort of this paper, however, only offers a

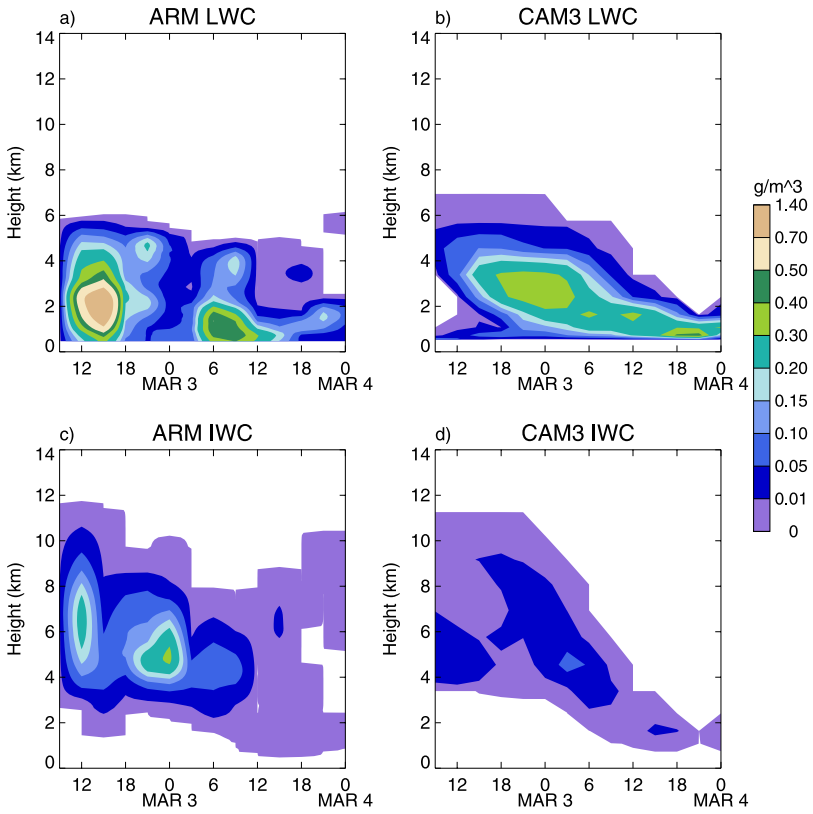

Figure 12. Same as Figure 9 except that CAM3 results are from sensitivity experiment.

snapshot at the process level to GCM biases. It is still an open question how representative is the bias of the dynamical circulation to climate models.

[38] **Acknowledgments.** The first author wishes to thank James Hack, Edmund Chang, Brian Colle, and Marvin Geller who provided valuable comments in the course of her Ph.D. research. We also wish to thank three anonymous reviewers whose detailed comments and suggestions have improved the paper significantly. This study is supported by the Atmospheric Radiation Measurement Program of the U.S. department of Energy. Additional support is by NASA and NSF to the Stony Brook University.

References

Bony, S., et al. (2006), How well do we understand and evaluate climate change feedback processes, *J. Clim.*, *19*, 3445–3482.

Boyle, J. S., D. Williamson, R. Cederwall, M. Fiorino, J. Hnilo, J. Olson, T. Phillips, G. Potter, and S. Xie (2005), Diagnosis of Community Atmospheric Model 2 (CAM2) in numerical weatter forecast configuration at Atmospheric Radiation Measurement sites, *J. Geophys. Res.*, *110*, D15S15, doi:10.1029/2004JD005042.

Carlson, T. N. (1980), Airflow through midlatitude cyclones and the comma cloud pattern, *Mon. Weather Rev.*, *108*, 1498–1509.

Cess, R. D., et al. (1990), Intercomparison and interpretation of climate feedback processes in 19 atmospheric general circulation models, *J. Geophys. Res.*, *95*, 16,601–16,615.

Clothiaux, E. E., et al. (2000), Objective determination of cloud heights and radar reflectivities using a combination of active remote sensors at the ARM CART sites, *J. Appl. Meteorol.*, *39*, 645–665.

Clothiaux, E. E., et al. (2001), The ARM millimeter wave cloud radars (MMCRs) and the active remote sensing of clouds (ARSCL) value added product (VAP), *DOE Tech. Memo. ARM VAP-002.1*, U.S. Dep. of Energy, Washington, D. C.

Collins, W. D., et al. (2006), The Community Climate System Model Version 3 (CCSM3), *J. Clim.*, *19*, 2122–2143.

Cubasch, U., et al. (2001), Projection of future climate change, in *Climate Change 2001: The Third IPCC Assessment Report*, pp. 528–582, Cambridge Univ. Press, New York.

Grumm, R. H. (1993), Characteristics of surface cyclone forecasts in the aviation run of the global spectral model, *Weather Forecasting*, *8*, 87–112.

Grumm, R. H., R. J. Oravec, and A. L. Siebers (1992), Systematic model forecast errors of surface cyclones in NMC's Nested-Grid Model, December 1988 through November 1990, *Weather Forecasting*, *7*, 65–87.

Junker, N. W., J. E. Hoke, and R. H. Grumm (1989), Performance of NMC's regional models, *Weather Forecasting*, *4*, 368–390.

Katzfey, J. J., and B. F. Ryan (1997), Modification of the thermodynamic structure of the lower troposphere by the evaporation of precipitation: A GEWEX cloud system study, *Mon. Weather Rev.*, *125*, 1431–1446.

Katzfey, J. J., and B. F. Ryan (2000), Mid-latitude frontal clouds: GCM-scale modeling implications, *J. Clim.*, *13*, 2729–2745.

Klein, S. A., and C. Jakob (1999), Validation and sensitivities of frontal clouds simulated by the ECMWF model, *Mon. Weather Rev.*, *127*, 2514–2531.

Liao, L., and K. Sassen (1994), Investigation of relationships between Ka-band radar reflectivity and ice and liquid water contents, *J. Atmos. Sci.*, *35*, 231–248.

Lin, W. Y., and M. H. Zhang (2004), Evaluation of clouds and their radiative effects simulated by the NCAR community atmospheric model CAM2 against satellite observations, *J. Clim.*, *17*, 3302–3318.

Liu, C. L., and A. J. Illingworth (2000), Toward more accurate retrievals of ice water content from radar measurements of clouds, *J. Appl. Meteorol.*, *39*, 1130–1146.

Miller, M. A., et al. (2003), ARM value-added cloud products: Description and status, paper presented at Thirteenth Atmospheric Radiation Measurement (ARM) Science Meeting, U.S. Dep. of Energy, Washington, D. C.

Minnis, P., D. P. Kratz, J. A. Coakley, M. D. King, D. Garber, P. Heck, S. Mayor, D. F. Young, and R. Arduini (1995), Clouds and the Earth's Radiant Energy System (CERES) algorithm theoretical basis document: Cloud optical property retrieval (subsystem 4.3), *NASA RP 1376*, 135–164.

Mullen, S. L., and B. B. Smith (1990), An analysis of sea-level cyclone errors in NMC's Nested Grid Model (NGM) during 1987–1988 winter season, *Weather Forecasting*, *5*, 433–447.

Norris, J. R., and C. P. Weaver (2001), Improved techniques for evaluating GCM cloudiness applied to the NCAR CCM3, *J. Clim.*, *14*, 2540–2550.

Oravec, R. J., and R. H. Grumm (1993), The prediction of rapidly deepening cyclones by NMC's Nested-Grid Model in winter 1989 through autumn 1991, *Weather Forecasting*, *8*, 248–270.

Rasch, P. J., and J. E. Kristjánsson (1998), A comparison of the CCM3 model climate using diagnosed and predicted condensate parameterizations, *J. Clim.*, *11*, 1587–1614.

Ryan, B. F., et al. (2000), Simulations of a cold front by cloud-resolving, limited-area, and large-scale models, and a model evaluation using in situ and satellite observations, *Mon. Weather Rev.*, *128*, 3218–3235.

Sanders, F. (1992), Skill of operational dynamical models in cyclone prediction out to five-day range during ERICA, *Weather Forecasting*, *7*, 3–25.

Sanders, F., and E. P. Auciello (1989), Skill in prediction of explosive cyclogenesis over the western North Atlantic Ocean, 1987/1988: A forecast checklist and NMC dynamical models, *Weather Forecasting*, *4*, 157–172.

Smith, B. B., and S. L. Mullen (1993), An evaluation of sea-level cyclone forecasts produced by NMC's Nested-Grid Model and Global Spectral Model, *Weather Forecasting*, *8*, 37–56.

Sundqvist, H. (1988), Parameterization of condensation and associated clouds in models for weather prediction and general circulation simulation, in *Physically-Based Modeling and Simulation of Climate and Climate Change*, vol. 1, edited by M. E. Schlesinger, pp. 433–461, Kluwer Acad., Norwell, Mass.

Tselioudis, G., and C. Jakob (2002), Evaluation of midlatitude cloud properties in a weather and a climate model: Dependence on dynamic regime and spatial resolution, *J. Geophys. Res.*, *107*(D24), 4781, doi:10.1029/2002JD002259.

Uccellini, L. W., P. J. Kocin, and J. M. Sienkiewicz (1999), Advances in forecasting extratropical cyclogenesis, in *The Life Cycles of Extratropical Cyclones*, pp. 317–336, Am. Meteorol. Soc., Boston, Mass.

U.S. Department of Energy (2006), Continuous profiles of cloud microphysical properties for the fixed atmospheric radiation measurement sites, *Rep. DOE/SC-ARM/P-0609*, Washington, D. C.

Webb, M., C. Senior, S. Bony, and J. J. Morcrette (2001), Combining ERBE and ISCCP data to assess clouds in the Hadley Centre, ECMWF and LMD atmospheric climate models, *Clim. Dyn.*, *17*, 905–922.

Xie, S., et al. (2005), Simulations of midlatitude frontal clouds by single-column and cloud-resolving models during the Atmospheric Radiation Measurement March 2000 cloud intensive operational period, *J. Geophys. Res.*, *110*, D15S03, doi:10.1029/2004JD005119.

Zhang, M. H., and J. L. Lin (1997), Constrained variational analysis of sounding data based on column-integrated budgets of mass, heat, moisture and momentum: Approach and application to ARM measurements, *J. Atmos. Sci.*, *54*, 1503–1524.

Zhang, M. H., J. L. Lin, R. T. Cederwall, J. J. Yio, and S. C. Xie (2001), Objective analysis of the ARM IOP data: Method and sensitivity, *Mon. Weather Rev.*, *129*, 295–311.

Zhang, M. H., et al. (2003), A modified formulation of fractional stratiform condensation rate in the NCAR community atmospheric model CAM2, *J. Geophys. Res.*, *108*(D1), 4035, doi:10.1029/2002JD002523.

Zhang, M. H., et al. (2005), Comparing clouds and their seasonal variations in 10 atmospheric general circulation models with satellite measurements, *J. Geophys. Res.*, *110*, D15S02, doi:10.1029/2004JD005021.

Zhang, Y.-C., W. B. Rossow, A. A. Lacis, V. Oinas, and M. I. Mishchenko (2004), Calculation of radiative fluxes from the surface to top of atmosphere based on ISCCP and other global data sets: Refinements of the radiative transfer model and the input data, *J. Geophys. Res.*, *109*, D19105, doi:10.1029/2003JD004457.

W. Lin, J. Wu, and M. Zhang, Institute for Terrestrial and Planetary Atmospheres, Marine Sciences Research Center, Stony Brook University, State University of New York, Stony Brook, NY 11794-5000, USA. (jwu@giss.nasa.gov)